

# Focused ion beam-shaped microtools for ultra-precision machining of cylindrical components

Y.N. Picard<sup>1</sup>, D.P. Adams\*, M.J. Vasile, M.B. Ritchey

Sandia National Laboratories, P.O. Box 5800, MS 0959, Albuquerque, NM 87185, USA

Received 23 April 2002; accepted 6 August 2002

## Abstract

Focused ion beam (FIB) sputtering is used to shape a variety of cutting tools with dimensions in the 15–100  $\mu\text{m}$  range and cutting edge radii of curvature of 40 nm. The shape of each microtool is controlled to a pre-specified geometry that includes rake and relief features. We demonstrate tools having rectangular, triangular, and other complex-shaped face designs. A double-triangle tip on one tool is unique and demonstrates the versatility of the fabrication process. The FIB technique allows observation of the tool during fabrication, and, thus, reproducible features are generated with sub-micron precision. Tools are made from tungsten carbide, high-speed tool steel, and single crystal diamond. Application of FIB-shaped tools in ultra-precision microgrooving tests shows that the cross-section of a machined groove is an excellent replication of the microtool face. Microgrooves on 40–150  $\mu\text{m}$  pitch are cut into 3 mm diameter polymer rods, for groove arc lengths greater than 12 cm. The surface finish of machined features is also reported; groove roughness ( $R_a$ ) is typically less than 0.2  $\mu\text{m}$ . Ultra-precision machining of cylindrical substrates is extended to make bound metal microcoils having feature sizes of 20–40  $\mu\text{m}$ .

© 2002 Elsevier Science Inc. All rights reserved.

*Keywords:* Focused ion beam; Microtool; Diamond tool; Microcoil; Ultra-precision machining

## 1. Introduction

Fabrication of microscale components with cylindrical symmetry is a significant challenge for prototyping and manufacturing. This is particularly difficult when using techniques that generate planar features, such as projection lithography.

Recent work, however, demonstrates processes that overcome some of the geometric limitations of conventional methods. Electronic devices are fabricated onto silicon substrates, such as spheres, using nontraditional lithographic techniques [1]. Microcontact printing on cylindrical surfaces with subsequent electrodeposition produces miniature 3-D structures with sub-micron resolution [2], and designed departures from the initial cylindrical geometry [3]. Serial processes such as laser chemical vapor deposition (CVD) [4] are used to deposit free-form helices from organic precursors, and laser stimulated exposure of resist-coated nonplanar substrates is also reported [5].

Despite progress with these recently developed techniques, many nonplanar geometries remain difficult to pattern. In particular, fabrication of cylindrical microscale components that have curved or nonrectilinear cross-section features is challenging. This includes, for example, helical threads on a cylinder that have triangular or trapezoidal feature cross-sections. Applications that require these geometries include microscrew components and precisely shaped knurling tools. Furthermore, most microfabrication techniques (e.g., electroplating, CVD) are capable of patterning a selected group of materials. Cylindrical components and devices require a diverse set of materials, including metals, alloys, polymers, and ceramics.

Ultra-precision machining techniques are capable of producing microscale structures with complex topology [6,7]. In particular, precision lathe machining is well-suited to cylindrical substrates or components, and many commercial instruments have nanometer-scale precision. However, one of the major difficulties with extending machining processes into the micron range (regardless of workpiece geometry) is the reliable fabrication of small cutting tools with the appropriate shape and dimensions [8]. Lu and Yoneyama [9] describe a micro-turning system and emphasize the need for miniaturization of cutting tools in order to achieve the

\* Corresponding author. Tel.: +1-505-844-8317; fax: +1-505-844-2754.

E-mail address: dpadams@sandia.gov (D.P. Adams).

<sup>1</sup> Present address: Department of Materials Science and Engineering, University of Michigan, Ann Arbor, MI, USA.

potential of the micro lathe. These authors adapt a diamond scanning probe microscope tip as the cutting tool, while others rely on standard diamond tools [10–12].

Other issues that arise with regard to the widespread applicability of ultra-precision machining using extremely small cutting tools include: the accuracy by which a microtool shape is transferred to the workpiece, the effects of friction/wear on a microtool, the strength and toughness of micron-size tools, the resultant polish of the machined feature (including debris) and the practical limits of feature size, pitch, and workpiece diameter.

Focused ion beam (FIB) sputtering is currently being researched as a method for fabricating microscopic cutting tools [13–18] with working dimensions in the tens of micron range. The use of these tools for machining metals, polymers, and ceramics is demonstrated in limited tests [16–18] with micromilling and with ultra-precision lathe turning. Development of machining techniques such as establishing the point of contact between the tool and workpiece, and determining reference positions also requires novel procedures, however, these are not as challenging as tool shaping. The major advantages to the FIB manufacture of microtools include: the variety of tool shapes, the control over tool geometry, the sub-micron dimensional resolution, and the observation of a tool during shaping. FIB sputtering creates tool shapes that cannot be fabricated easily by conventional techniques such as polishing and grinding. Also, this technique is beneficial for shaping tools, because negligible mechanical force is placed on the tool during FIB fabrication. Tools are shaped by an atom-by-atom removal process.

This report is concerned with cutting tools for ultra-precision lathe turning of grooves on cylinders or other rotationally symmetric shapes. The object is to transfer the tool face shape to the workpiece. The immediate applications include extremely small solenoids and the rotary element of a microscrew pump. Microcoils and microsolenoids are good examples of a structure type that is characteristically hard to produce by classical methods. A process consisting of machining (to define features) and metal deposition has the potential to produce small diameter solenoids with a large number of turns per unit length. Small solenoids have proven very tedious to manufacture by winding techniques, particularly for conductor diameters of 25  $\mu\text{m}$ .

## 2. Microtool fabrication by focused ion beam sputtering

Starting materials for microtool fabrication are commercially supplied, generally in the form of a tapered cylinder attached to a 3.175 mm diameter mandrel. The total length of the tool shank and mandrel is approximately 2.5 cm. High-speed steel and tungsten carbide tool blanks are available from National Jet, Co. as micro-punches. The final 25–120  $\mu\text{m}$  length of the shank is uniform at the specified diameter. Tapered single crystal diamond tool blanks are obtained from Microstar, Inc. The final segment of diamond

tool blanks is  $\sim 150 \mu\text{m}$  long with an approximate 40  $\mu\text{m}$  square cross-section.

The FIB system used to shape micro-cutting tools is described in detail elsewhere [19,20]. In general, it is a high vacuum apparatus that accelerates and directs ions at a target material. Material is removed by physical sputtering, and the secondary electrons emitted during this process are collected to form an image of the sample. A tool blank is mounted on an X–Y stage having sub-micron motion resolution, and full 360° rotational motion is available to the tool blank with 0.37° increments. Fig. 1 illustrates the orientation of a tool blank with respect to the ion beam (indicated by an arrow), and the removal of segments of a cylindrical tool by sputtering. The microtool depicted in Fig. 1 has two cutting faces and is modeled for ultra-precision turning applications. The beam used to shape tools is 20 keV ionized gallium with a spot size of 0.5  $\mu\text{m}$ , and 2 nA total current (as measured in a Faraday cup). The sputter pattern is generated on a bit plane image of the tool end, and can have virtually any shape. This pattern is recorded and transferred to the ion beam deflection system, resulting in a shape in the tool that replicates the pattern. Once all the required facets are ion milled for a given starting rotational position, a tool is rotated to a different orientation, and the process is repeated. Judicious choice of the FIB milling and rotation sequence produces a tool with the target rake angles and extremely sharp cutting edges.

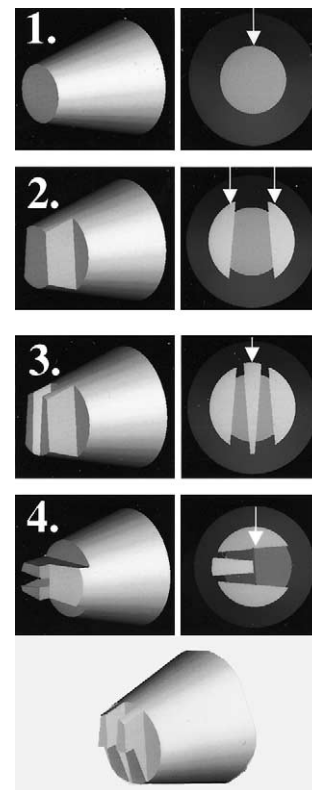


Fig. 1. Procedure for ion milling (shaping) a micro-threading tool. For all sputter steps, a tool is fixed. Arrows indicate the direction of the ion beam. A completed two-tip design is shown at bottom.

Table 1  
Metrology of FIB-shaped microtools prior to ultra-precision machining

Tool material	Cutting edge radius of curvature (nm)	Cutting edge roughness, PV, $R_a$ ( $\mu\text{m}$ )	Facet roughness, $R_{\text{rms}}$ , $R_a$ ( $\mu\text{m}$ )	Taper angle of a single facet created by ion beam ( $^\circ$ )
C2 WC:Co	40	0.15, 0.05	0.14, 0.04	3.0
M42 HSS	N/M	0.11, 0.05	0.13, 0.05	4.1
Diamond	40	0.12, 0.04	0.15, 0.09	2.0

HSS, high-speed steel; WC:Co, cemented tungsten carbide; PV, the peak-to-valley height;  $R_a$ , the roughness average; and  $R_{\text{rms}}$ , the root-mean-square average.

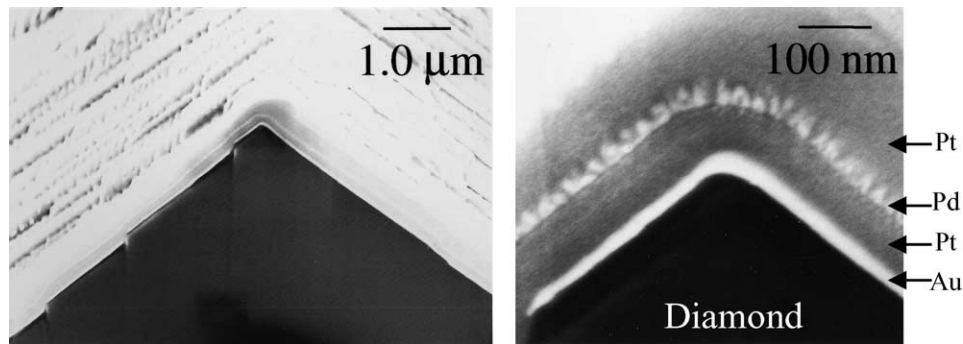


Fig. 2. Scanning electron microscope images of a diamond microtool cutting edge. The edge is formed by FIB sputtering two facets at a relative angle of  $\sim 100^\circ$ . The lower magnification image (left) shows a perspective view of the edge of intersection and a portion of the ion beam milled facets. Several metal layers are also shown in the cross-section image on right. These protect the diamond during sample thinning and make the sample conductive for SEM. The higher magnification image (right) is used for determining radius of curvature and is, therefore, aligned with the tool axis.

As discussed previously [13–15], a particular ion–solid orientation is used to create sharp cutting edges. With the FIB stage and tool fixed, the gallium beam impinges normal to a plane containing the tool axis. This geometry is ideal for creating one sharp cutting edge per facet on the side furthest from the ion source. The facet edge closest to the ion source is rounded, because a part of the Gaussian beam intensity extends outside the user-defined pattern boundary. In addition, a grazing-incidence geometry employed as a final polish step for each facet minimizes the effects of ion implantation and modifications to tool microstructure, particularly at the far edge of the facet designated for cutting. Transmission electron microscopy reveals that the beam induced changes to tool microstructure are restricted to a 10 nm depth or less when using a 20 keV energy [21].

The tool materials selected for this study include M42 high-speed steel, C2 grade tungsten carbide, and single crystal diamond. With regard to the FIB fabrication process, the steel and carbide require the smallest time for shaping. A 25  $\mu\text{m}$  wide threading tool made of steel or carbide can be fabricated in 3–5 h using a 2.0 nA ion beam. Note, use of a commercial 20 nA ion source would reduce the fabrication time to less than 30 min for most tool geometries described in this report. Diamond, on the other hand, requires significantly longer time owing to a relatively high C–C surface binding energy. Despite the slow rate of shaping, we pursue processes that sculpt diamond because these tools are compositionally homogeneous. It is expected that homogeneous materials could be shaped to extremely small dimensions and maintain suitable mechanical properties required for cutting,

compared with particular grades of cemented carbide and steels that have relatively large microstructural features and are inhomogeneous.

All three tool materials have several similar characteristics when shaped by FIBs. Characteristic features analyzed include the cutting edge radius of curvature, the cutting edge roughness, the facet roughness, and the taper angle formed behind a cutting edge for different tool materials. A summary of FIB-shaped microtool features is presented in Table 1.

In general, the tool cutting edges are extremely sharp. We measure the cutting edge radii of curvature to be 40 nm for diamond and tungsten carbide. Measurements of cutting edge radii of curvature involve initially sputtering two facets onto a tool blank using the FIB system. The two facets are oriented so that they intersect along an edge. The edge of intersection is then cross-sectioned by a second FIB system and viewed at a magnification of 200,000 $\times$  in a field emission scanning electron microscope to determine radius of curvature. A representative scanning electron micrograph of a diamond cutting edge is shown in Fig. 2. Care is taken to prevent the specimen preparation procedure from affecting the measurement.<sup>2</sup>

<sup>2</sup> Sample preparation for electron microscopy involved deposition of a protective Au metal film onto the microtool using electron beam evaporation. The sample was then coated with a Pt–C layer by electron beam CVD. Additional layers include Pd (used as a marker) and a relatively thick Pt–C layer deposited by FIB–CVD. The deposited metals protect the tool edge morphology during ion beam thinning and prevent charging in the electron microscope. A single region is sputtered along the edge of intersection using a different focused ion beam sputter system (FEI DB235).

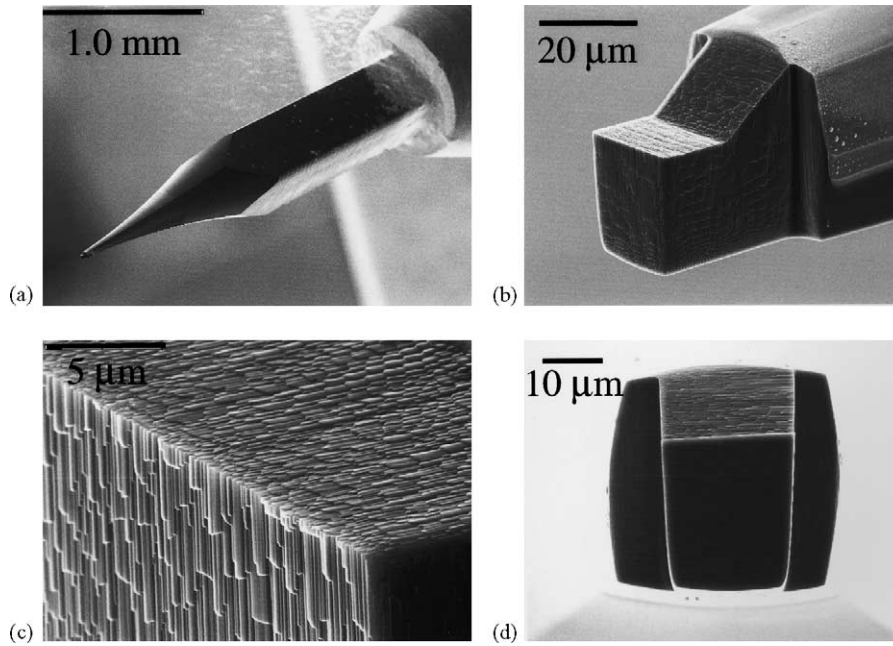


Fig. 3. (a) Low magnification view of a single crystal diamond tool shank and junction with mandrel. The tool cutting edges are fabricated on the last  $\sim 30 \mu\text{m}$  near the tip. (b) Perspective-view, high magnification scanning electron micrograph of the same diamond tool showing the FIB-shaped facets. (c) Left side cutting edge of same microtool. This image shows the intersection of three FIB-sputtered facets. (d) End view of the tool.

In addition to extremely small cutting edge radii of curvature, all tools have a small cutting edge roughness as determined from scanning electron microscopy (SEM). Using SEM, we obtain an image of the edge joining two FIB-sputtered facets by viewing perpendicular to the edge of interest. Afterwards, SEM micrographs are scanned by a microdensitometer, and the fluctuations in height are analyzed to determine a line roughness. In general, all tool materials show a cutting edge roughness ( $R_a$ ) of  $0.05 \mu\text{m}$  or less. The peak-to-valley heights along edges are listed in Table 1 and are less than or equal to  $0.15 \mu\text{m}$ .

Facet roughness is also measured for each tool material, and, not surprisingly, this is similar in magnitude to the cutting edge roughness. A calibrated ADE Phase Shift MicroXAM white light interferometric microscope having a vertical (height) resolution of  $0.8 \text{ \AA}$  is used to quantify facet roughness. In general, the  $R_a$  of FIB-sputtered facets is  $0.04\text{--}0.09 \mu\text{m}$  when measurements are taken away from the facet edges. The facet roughness values listed in Table 1 are comparable with measurements taken from the tools shown in Figs. 3–5. Facets are extremely smooth but have noticeable nanometer-size steps and ripples that form

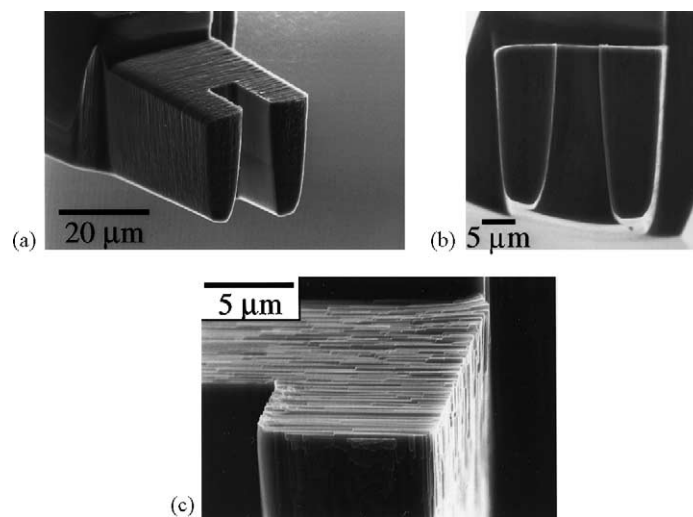


Fig. 4. (a) Two tip, single crystal diamond tool shaped by FIB sputtering. (b) End view of the same tool demonstrating relief behind cutting edges. (c) High magnification view of a single tip of this two tip tool.

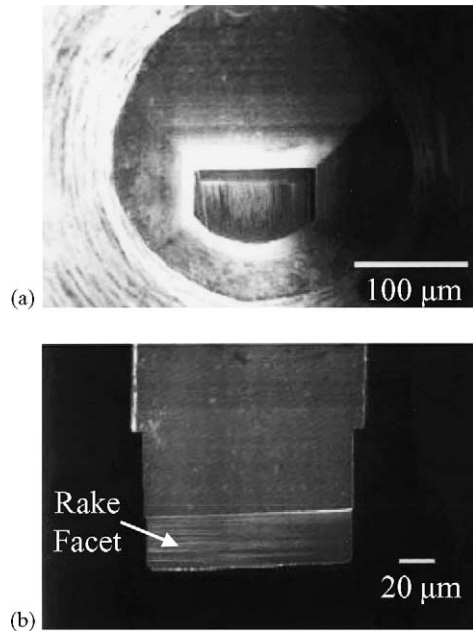


Fig. 5. Custom-ground tool after shaping by ion sputtering. Images show a view along the tool axis (a) and perpendicular to the tool face (b). Ions are used to define sharp cutting edges, relief and a rake facet.

across the surface when viewed at high magnification using SEM.

When shaping a microtool by FIB sputtering, it is important to recognize that each facet sputtered onto a cylindrical tool blank has a normal direction that is not perpendicular to the ion beam vector. In other words, facets are tapered, as shown in Fig. 1. Typically facets are oriented  $2\text{--}4^\circ$  with respect to the ion beam depending on the tool material (see Table 1). The taper angle formed is a result of the physics of the ion–solid interaction. Specifically, ions impinging at near glancing angles most often reflect without displacing atoms from lattice sites. The taper angle resulting from FIB shaping is measured by viewing down the axis of a  $25\ \mu\text{m}$  wide tool using SEM. Tools used for this measurement have two nonintersecting facets that are sputtered using a single tool orientation (as shown in Fig. 1, step 2). The taper angle generated by the FIB process is measured for each tool material, so that a tool's relief and side rake angles can be tailored to within  $\sim 0.5^\circ$  by the operator. With our FIB system, the stage can rotate a tool to a different orientation prior to sputtering of individual facets.

### 3. Diamond microtools

A micro lathe tool that has been ion milled from a diamond tool blank is shown in Fig. 3. The starting material is a single crystal segment that is brazed into a tapered tungsten carbide mandrel, and ground to an approximate  $40\ \mu\text{m} \times 40\ \mu\text{m}$  square cross-section. The width of the tool after ion shaping is  $23\ \mu\text{m}$ . A cutting edge formed by the intersection of

two ion-milled facets is shown at higher magnification in Fig. 3(c). This edge has a roughness ( $R_a$ ) of  $0.04\ \mu\text{m}$  and a radius of curvature equal to  $40\ \text{nm}$ . The shingled appearance of the FIB-sputtered diamond surfaces shown in Fig. 3(b) and (c) is composed of nanometer-size microfacets that form as a result of ion beam bombardment at near-grazing incidence angles. We expect that these features form as a result of a well-documented sputter-induced morphological instability [22] and related phenomena [23].

The end view of the diamond tool is shown in Fig. 3(d). This tool is made to have a small side rake angle ( $2.0^\circ$ ) and relief behind all cutting edges. The fact that the material is single crystal diamond has little effect on the final geometry of the tool; however, the ion-milling rate is significantly lower than that for steel or tungsten carbide as described previously.

Fig. 4 demonstrates the ability to tailor tool geometry by the FIB fabrication process. The tool shown in Fig. 4 is also shaped from a single crystal diamond blank, but the ion-milling patterns and sequences are chosen so that two rectangular cutting surfaces with  $10\ \mu\text{m}$  wide tips separated by  $7.7\ \mu\text{m}$  result. In general, any complex tool face geometry is possible.

Each of the tips on the tool shown in Fig. 4 measure  $10\ \mu\text{m}$  (wide)  $\times$   $12\ \mu\text{m}$  (long). The right tip in Fig. 4(b) is  $29\ \mu\text{m}$  thick, while the left tip is  $26.5\ \mu\text{m}$  thick. The variation in thickness is a result of the original cross-section of the tool blank, and its orientation to the ion beam. Nevertheless, relief is established behind all cutting edges on this two-tip tool. It is expected that shaping of similar two-tip diamond tools on this scale would be virtually impossible by conventional methods such as grinding.

## 4. Specialized high-speed steel tools

Two tool sizes are selected for making high-speed steel lathe cutting tools for different applications. The first application is the production of a cylinder with relatively wide rectangular cross-section grooves. The second application is the production of an ultra-fine triangular groove pair on a cylinder.

### 4.1. Rectangular cross-section grooves

The rectangular cross-section grooves for the first application are large, having a  $95\ \mu\text{m}$  (width)  $\times$   $45\ \mu\text{m}$  (depth)  $\times$   $150\ \mu\text{m}$  (pitch). A set of tool blanks that are custom ground to dimensions slightly larger than the final tool size is obtained, and the cutting edges and the rake angles are finished by FIB. The result of shaping a custom-ground tool by FIB is shown in Fig. 5(a) and (b). The new sidewalls are separated by  $94.9\ \mu\text{m}$  for a length of  $70\ \mu\text{m}$ , and the cutting edges have a relief angle of  $4.2^\circ$ . The tool-end cutting edge is also sharpened by ion milling, and a rake facet is defined by FIB.

The tool shown in Fig. 5 is measured for the sharpness of the cutting edges prior to machining. The cutting edge

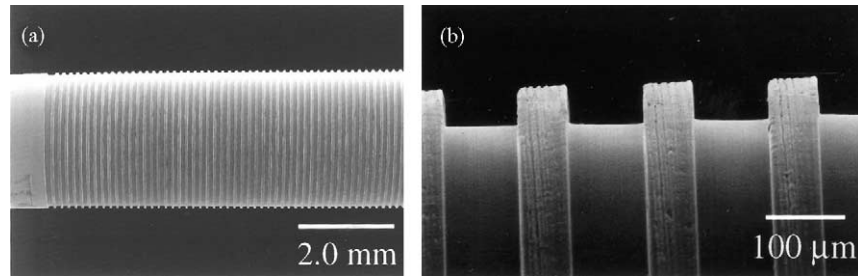


Fig. 6. Groove machined in PEEK using FIB-polished, custom-ground lathe tool. (a) Shows an image of the groove ending in a circumferential ring. (b) Shows a high magnification view of the smooth helical feature.

radii are less than  $1 \mu\text{m}$ , as determined by scanning electron microscope views at a magnification of  $200,000\times$ .

Each custom-ground tool shaped by FIB cut one or more helical grooves in polyether etherketone (PEEK) cylinders. A portion of a PEEK cylinder is mounted in the chuck of an ultra-precision PreciTech lathe (Optimum 2000), with one free end. Each PEEK cylinder surface is cut true with a commercially supplied diamond tool. After polishing, PEEK workpieces have a 3 mm diameter and a total cylinder length of 2.0 cm. The FIB-shaped microtool is then brought towards the workpiece surface, and contact is made with the sample as observed through an optical microscope. Multiple passes are made to achieve the final depth; a typical depth per pass is  $2 \mu\text{m}$  or less. Grooves are cut at 500 rpm rotation, and at a longitudinal travel rate of 1.25 mm/s. The depth cut per pass and the final depth are programmed prior to operation, and the instrument controls rotational alignment and z-axis positioning to allow for accurate machining of a helix.

Fig. 6 shows portions of a groove cut in a PEEK cylinder. The groove consists of a long helix with a ring at both ends. Each ring is cut to the depth of the helix. The helical portion of the groove begins at a distance of 2.55 mm from the lathe chuck. A portion of the helix is shown in Fig. 6(b), demonstrating smooth groove bottom and sidewall surfaces.

We find that for 3 mm diameter PEEK rods cut by tools such as the one shown in Fig. 5, the groove dimensions are close to the intended values. Measurements of groove depth, width, and pitch are made over arc lengths of 225 mm, corresponding to a cylinder length of 3.8 mm. Metrology using SEM includes four measurements on each helical turn, taken in  $90^\circ$  increments. In summary, we find that the width of the helical groove shown in Fig. 6 is  $94.6 \mu\text{m}$  with a standard deviation of  $0.63 \mu\text{m}$ . The groove depth is  $44.6 \mu\text{m}$  with a standard deviation of  $2.3 \mu\text{m}$ . The roughness of the machined feature bottom is determined by white light interferometry to be  $0.22 \mu\text{m}$  ( $R_{\text{rms}}$ ) and  $0.14 \mu\text{m}$  ( $R_a$ ). A table at the end of this paper summarizes results from all ultra-precision machining tests using FIB-shaped tools.

Beyond cylinder lengths of  $\sim 4.0$  mm the FIB-polished microtool significantly deflects the workpiece, and as a result the groove depth deviates by  $\geq 10\%$  of the intended value. Evidence of a rough surface finish created during a polish step can also be found at these lengths, most likely due to

chatter. It is expected that grooves of constant depth can be made substantially longer by using a tail stock for workpiece support.

Two PEEK cylinders are cut with the tool shown in Fig. 5, and the material volume removed from each is  $4.5 \times 10^{-3} \text{ cm}^3$ . The tool edges are inspected after cutting each PEEK cylinder to ensure that the tool remained sharp. The tool cutting edge radii increased no more than  $0.1 \mu\text{m}$  after the second grooving operation.

#### 4.2. Double triangle grooves

The second application of high-speed steel tools includes machining a pair of closely spaced triangular grooves into the surface of a 3-mm diameter PEEK rod using a two-tip tool. This tests both the ability of FIB to make a two-tip tool having a nonrectilinear tool face shape and the ability of a lathe machine to position a microtool along the z-axis of the cylinder and to maintain rotational alignment. Ultra-precision machining with this tool involves multiple passes, whereby the tool is reengaged several times at the origin of cut.

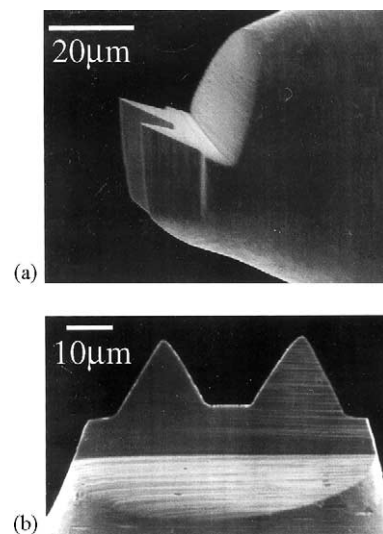


Fig. 7. Two-tip microtool having triangular cutting faces. Tool is made of M42 high-speed steel and is shaped by FIB sputtering. Image in (b) shows the cutting face.

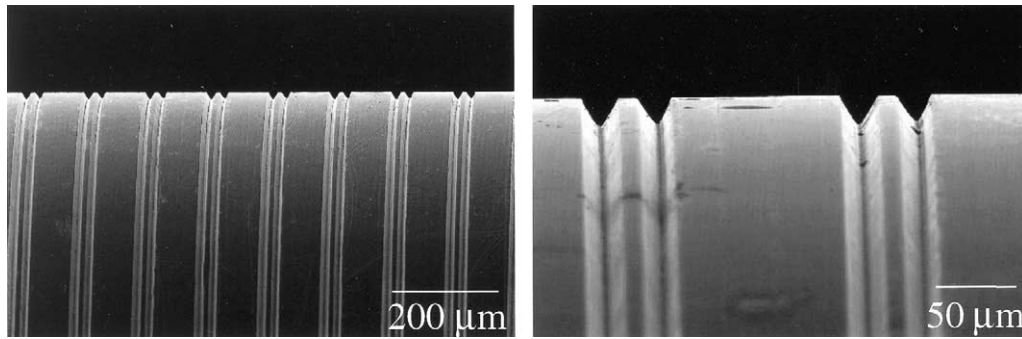


Fig. 8. A portion of the PEEK workpiece machined using the FIB-shaped, two-tip tool shown in Fig. 7.

Fig. 7 shows two views of a high-speed steel two-tip tool, before lathe machining. Each tip face is triangular and has an included angle of  $62.5^\circ$  as shown in Fig. 7(b). A back rake angle of  $10^\circ$  is also created for both tips. A relief angle of approximately  $4^\circ$  is established behind all cutting edges and behind the two end points of the tool. The two tips are  $24\ \mu\text{m}$  long.

Fig. 8 shows a portion of the triangular grooves cut into 3 mm diameter PEEK rod using the tool shown in Fig. 7. Qualitatively, the tool shape appears to be replicated very well in the cross-section of the grooves indicating that the Optimum 2000 lathe does an excellent job of managing rotational alignment and  $z$ -axis control. Both grooves in Fig. 8 have an angle of approximately  $62.5^\circ$ . The depths of the two grooves are also similar and close to the intended depths,  $\sim 15\ \mu\text{m}$ . The pitch of the groove pair is  $150\ \mu\text{m}$ , and the total arc length of each groove is 18 cm.

Measuring both the groove angle and the groove depth as a function of arc length has made a more stringent evaluation possible. Fig. 9 shows the measurements of depth and angle at the beginning of a helix, and after numerous turns. This includes measurements made at  $90^\circ$  increments per helical turn. In general, Fig. 9 demonstrates that both the angle and depth are virtually independent of rotational position around the circumference. This consistency owes to the precision of the machine, the ability to make a workpiece round on the lathe prior to groove definition, and the lack of workpiece deflection by the FIB-shaped microtool for large cylinder lengths. This particular tool leads to far less workpiece de-

flection than the larger tool shown in Fig. 5, and no change in groove depth is observed along the entire machined cylinder length.

In Table 2, we summarize the characteristics of several lathe machined grooves. In general, there is excellent matching between the target groove dimensions and the measured values. The widths and cross-sectional shapes of the machined features are nearly identical to that of the microtool face as evaluated using SEM. This matching continues for many turns along the cylindrical workpieces. The groove arc lengths listed are those over which the features remained uniform and, in some cases, the total length. However, there is reason to expect that uniform features could be machined to much greater lengths with workpiece support.

Tool dimensions, groove widths and groove depths are measured using SEM. In order to determine groove dimensions, the workpiece is positioned so that the cross-section of a groove can be viewed. Multiple turns are analyzed to determine average depth and width including measurements for different quadrants of rotation. A calibrated ADE Phase Shift MicroXAM white light interferometric microscope is used for measurements of groove roughness for those helical features having a rectangular cross-section. As mentioned previously, this instrument has a vertical (height) resolution of  $0.8\ \text{\AA}$  in the mode used for analysis. Workpiece cylindricalness is removed to allow for an accurate determination of roughness along the groove bottom. PEEK samples are insufficiently reflective for measurement by the interferometer. These require a thin layer ( $\sim 15\ \text{nm}$ ) of Au/Pd.

Table 2  
Results from threading different workpieces with FIB-shaped microtools

Workpiece material (diameter, mm)	Groove length (mm)	Tool face shape	Tool face angle ( $^\circ$ )	Groove angle (S.D., $^\circ$ )	Tool width ( $\mu\text{m}$ )	Groove width (S.D., $\mu\text{m}$ )	Target depth ( $\mu\text{m}$ )	Groove depth (S.D., $\mu\text{m}$ )	Groove roughness ( $R_{\text{rms}}$ , $R_a$ , $\mu\text{m}$ )
PEEK (3.00)	225	Rectangle	90	90 (0.4)	94.9	94.6 (0.63)	45.0	44.6 (2.3)	0.22, 0.14
PEEK (3.00)	219	Rectangle	90	90 (0.4)	92.9	92.1 (0.5)	45.0	45.7 (1.4)	0.16, 0.13
Cu/PMMA (3.00)	377	Rectangle	90	90 (0.2)	19.0	19.3 (0.2)	15.0	15.2 (0.5)	0.25, 0.20
PEEK (3.00)	140	Triangle	62.5	62.65 (0.49)	20.0	19.9 (0.1)	15.5	15.67 (0.47)	N/M
PEEK (3.00)	140	Triangle	62.5	63.10 (0.80)	18.4	18.5 (0.1)	14.0	14.25 (0.54)	N/M

Tool width for the triangular shaped microtools is defined as the width of the tool face at a distance from the tool end equal to the target groove depth. Roughness is measured on the bottom of a machined groove. N/M, not measured.

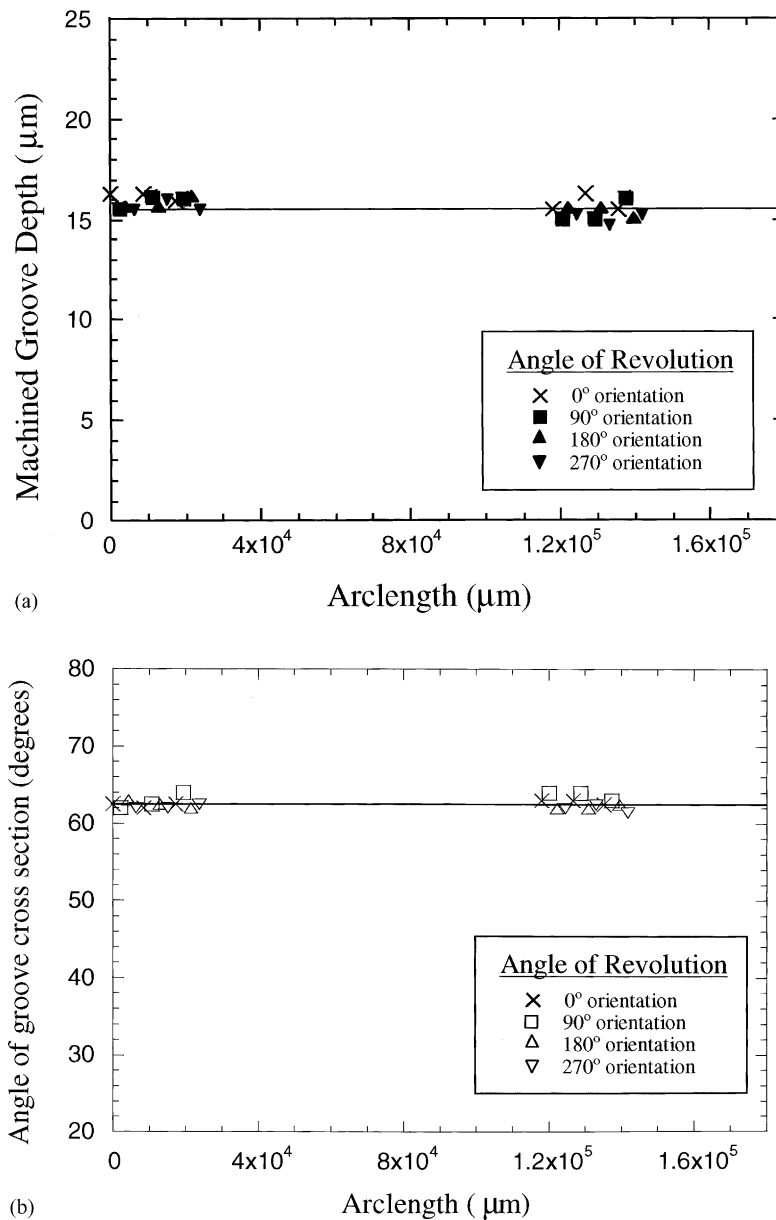


Fig. 9. Plots of (a) machined groove depth and (b) groove cross-section angle. Data is obtained from an ultra-precision machined PEEK cylinder and is plotted as a function of the groove arc length for different workpiece rotation quadrants.

## 5. Fabrication of miniature solenoids

Miniature electric windings or solenoids formed on cylinders of 3 mm diameter or less with conductor cross-section dimensions on the order of 25  $\mu\text{m}$  are extremely painstaking to fabricate by hand wrapping and have low yield. Therefore, a variety of processes are being investigated to make high winding density microcoils for use as magnetic actuators, transformers, and sensors [24–28]. Processes researched to date include soft lithography [26], LIGA<sup>3</sup> [28], wire wrapping by automated devices [29], and CVD [4].

<sup>3</sup> LIGA is an acronym for lithographie-galvanoformung-abformung.

In this report, we describe two different processes for fabricating microcoil structures that could find use in prototyping or small-lot production. These processes take advantage of the FIB tool shaping and the precise lathe micromachining techniques described in previous sections. We combine these ultra-precision machining techniques with thin film vapor deposition and electroplating.

The first process involves coating a cylindrical-shaped polymer such as polymethyl methacrylate (PMMA) or PEEK. As an example, we use a 20  $\mu\text{m}$  thick Cu conducting layer that is deposited by electron beam evaporation and subsequent electroplating. A FIB-shaped tool is then employed in a precision lathe to cut the conductive layer in

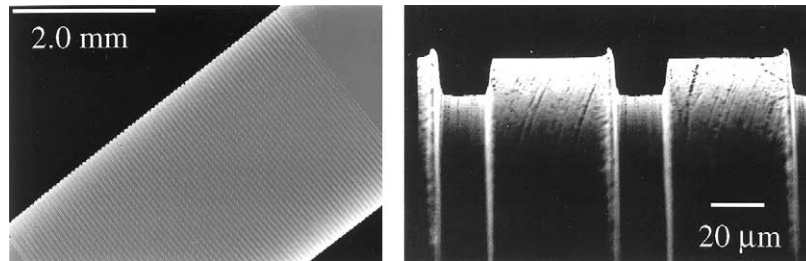


Fig. 10. Images of a single thin film coil bound to a PMMA cylindrical substrate. Component is made by depositing a Cu film followed by ultra-precision lathe machining.

sequentially increasing depths until the (soft) insulating support is reached. The result is an electrically isolated helical winding in which the conductor width is determined by the pitch of the micro-turning operation. The thickness of the metal conductor is set by the electroplating procedure and etching (if removal of debris is deemed necessary). Areas at both ends of a helical cut serve as rigid contact cuffs for wire bonding.

Fig. 10 shows the helical cut in a copper coating on a 3.0 mm diameter PMMA rod. This helix has a pitch of  $74\ \mu\text{m}$ , leaving a conductor with a rectangular cross-section of  $45\ \mu\text{m} \times 15\ \mu\text{m}$ . Samples can be cleaned to remove debris by brushing or etching.

The second coil fabrication method is essentially an adaptation of the Damascene [30] process used on planar substrates for microelectronics. In our experiments, a 1.0 mm diameter Macor rod is chosen as the insulating substrate, and  $20\ \mu\text{m}$  wide grooves are machined into the surface using a FIB-made tool to a depth of  $20\ \mu\text{m}$ , with a pitch of  $70\ \mu\text{m}$ . The repeated pattern consists of five helical turns as shown in Fig. 11(a). The substrate is then coated with vacuum evaporated Cr to promote adhesion followed by a seed layer of Cu. Subsequently, the sample is electroplated with Cu to a thickness that exceeded the original diameter of the Macor cylinder. A mechanical polish removes the excess copper until the underlying Macor support is exposed. The result, shown in Fig. 11(b), is electroplated copper windings contained on a machined Macor cylinder, with each conduct-

ing path separated by insulating ceramic. Helical segments shown in Fig. 11 are separated by  $200\ \mu\text{m}$  long copper contact areas (cuffs). These are areas machined during the same ultra-precision lathe turning process. Metal films are plated into these areas for the purpose of wire bonding.

## 6. Summary and future work

This work successfully extends conventional lathe machining techniques to the microscale in order to fabricate a variety of cylindrical components. In general, we demonstrate methods that allow for control of feature cross-section. This includes the ability to tailor nonrectilinear feature shapes uniformly around the circumference of a workpiece.

FIB sputtering is used to precisely shape micro-threading tools that have well-defined back and side rake angles, cutting edge widths and relief. A particular ion beam sample orientation used during microtool shaping is responsible for generating extremely sharp cutting edges. This orientation is particularly useful for shaping edges in compositionally inhomogeneous materials such as cemented carbide and tool steel. The cutting edge roughness of M42 high-speed tool steel, diamond and C2 tungsten carbide tools is measured to be  $0.05\ \mu\text{m}$  or less. The cutting edge radius of curvature is also a small fraction of the microtool width and length, making the cutting edge sharp compared to the depth per pass used during machining (typically  $2\ \mu\text{m}$  in this study).

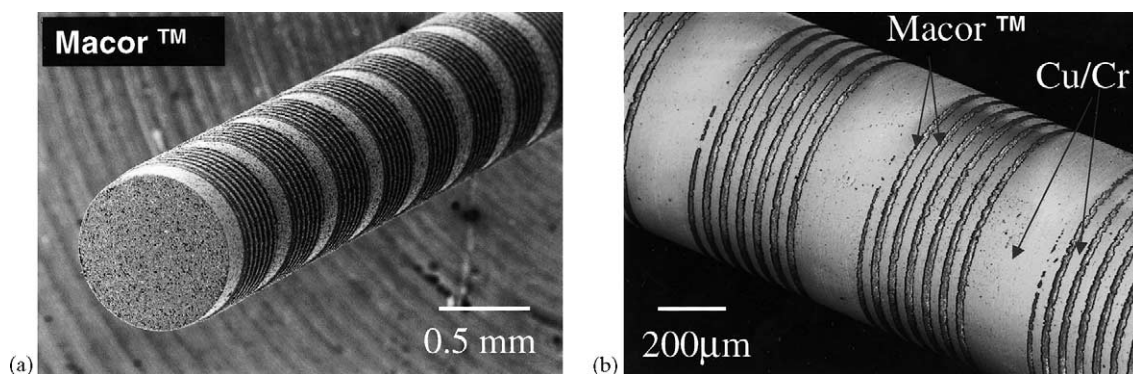


Fig. 11. Two stages of the Damascene process used to make thin film microcoils. Helical grooves are patterned by ultra-precision machining as shown in (a). Afterwards, Cr/Cu seed layers are deposited, and electroplating is used to thicken the metal. Polishing after deposition and plating results in a completed microcoil shown in (b).

SEM reveals that tools have cutting edge radii of curvature equal to 40 nm or less.

FIB sputtering has the advantage that almost any conceivable microtool geometry can be fabricated on a scale that is below those reached by grinding methods. This includes the potential fabrication of tools with curved shapes. We demonstrate the advantages of FIB sputtering in this paper by showing microtools with multiple tips separated by small gaps. Tools with nonrectilinear face shapes are shown including triangular tools. These tools are subsequently used to define features on cylindrical components by ultra-precision machining. In general, machined feature cross-sections closely match tool face shape. Metrology of machined workpieces shows nearly identical feature widths and included angles compared with the fabricated microtools. Measurements of groove depth around the circumference of cylindrical workpieces show good matching independent of arc length, thus demonstrating the ability of precision lathe machines to fabricate microscale and miniature cylindrical components. Additional work takes advantage of the ability to define a precise helix and fabricates thin film microcoils with 25  $\mu\text{m}$  wide metal turns.

Although FIB sputtering is a relatively slow process compared with other techniques, we envision that a high yield tool-making process with reasonable throughput can be achieved using existing FIB technology. FIB sputtering imposes no large forces on the tool during fabrication; material is removed atom-by-atom. Therefore, it is unlikely that a tool will be broken during fabrication. In terms of the time required for fabrication, a FIB column capable of producing 20 nA current (compared with our 2 nA beam) would allow for fabrication of a 25  $\mu\text{m}$  wide high-speed steel and tungsten carbide tool in less than 30 min.

Diamond cutting tools shaped by FIB sputtering are also demonstrated in this report with extremely precise dimensions and complex tool face shapes, but greater fabrication times are required compared with the other two materials studied. In general, a diamond tool can be made to have rake, relief, minimal cutting edge roughness, and an extremely small radius of curvature ( $\sim 40$  nm), but these tools require many hours of sputtering. Nevertheless, recent studies [31] demonstrate a modification to the current technique, known as gas-assisted FIB sputtering, that should reduce the required time to shape a tool. Based on known effects of  $\text{H}_2\text{O}$ -assisted sputtering [32] of diamond, it is reasonable to expect that our process for shaping a 25  $\mu\text{m}$  wide diamond tool can be modified to relatively short time (30 min or less) when using a 20 nA beam. Future research must examine the effects of different rate-enhancing ‘assist gases’ on microtool cutting edge roughness and radius of curvature.

## Acknowledgments

The authors appreciate the efforts of J. Michael (SNL), V. Carter Hodges (SNL), and S. Moncrief at Louisiana Tech

University (Ruston, LA). This work is supported by the United States Department of Energy under Contract No. DE-AC04-94AL85000. Sandia is a multiprogram laboratory operated by Sandia Corporation, a Lockheed Martin Company, for the United States Department of Energy.

## References

- [1] Ball Semiconductor, Inc., Allen, Texas 75013 [see examples].
- [2] Jackman RJ, Brittain ST, Adams A, Prentiss MG, Whitesides GM. Design and fabrication of topologically complex, three-dimensional microstructures. *Science* 1998;280:2089–91.
- [3] Brittain ST, Schueller OJA, Wu HK, Whitesides S, Whitesides GM. Microorigami: fabrication of small, three-dimensional, metallic structures. *J Phys Chem B* 2001;105(2):347–50.
- [4] Maxwell J, Larsson K, Boman M, Hooge P, Williams K, Coane P. Rapid prototyping of functional three dimensional microsolenoids and electromagnets by high-pressure laser chemical vapor deposition. *Proc Solid Freeform Fabrication Symp* 1998;529–36.
- [5] Trenkel C, Hammond GD, Speake CC. Photolithographic manufacture of a superconducting levitation coil on a spherical substrate. *Prec Eng* 1999;24:139–45; Lullo G, Arnone C, Giaconia C. Technologies for the fabrication of cylindrical fine line devices. *Microelectron Eng* 1997;35:417–20.
- [6] Weule H, Huntrup V, Tritschler H. Micro-cutting of steel to meet new requirements in miniaturization. *Ann CIRP* 2001;50:61.
- [7] Schaller T, Bohn L, Mayer K, Schubert K. Microstructure, grooves with a width of less than 50  $\mu\text{m}$  cut with ground hard metal micro end mills. *Prec Eng* 1999;234:229–35; Schaller T, Schubert K. Micromachining by CNC slotting using a standard tool. *ASPE Proc* 2001;25:469–77.
- [8] Hoffmeister H-W, Wenda A, Herrman H. The fabrication of micro milling cutters. In: *Proceedings of the International Conference on Microtechnologies: Microtec*, Hanover, Germany, 2000 Sept 25–27; 2000, p. 125–9.
- [9] Lu Z, Yoneyama T. Micro cutting in the micro lathe turning system. *Int J Machine Tools Manufact* 1999;39:1171–83.
- [10] Okazaki Y, Kitahara T. NC Micro-lathe to machine micro-parts. *ASPE Proc* 2000;22:575–8.
- [11] Bohart A, Collins P, Faulk S, Halvorson C, McClellan M, Shillito K. Affordable, compact, research single point diamond turning machine. *ASPE Proc* 2000;22:184–6.
- [12] Clarke M, Pierser M, Knuefermann M, Read R. New technology and novel design make sub-micron production practical. *ASPE Proc* 2000;22:187.
- [13] Vasile M, Friedrich C, Kikkeri B, McElhannon R. Micrometer scale machining: tool fabrication and initial results. *Prec Eng* 1996;19:180–6.
- [14] Friedrich C, Vasile M. Development of the micromilling process for high aspect ratio microstructures. *J Microelectromech Syst* 1996;5:33–8.
- [15] Friedrich C, Vasile M. Micromilling development and applications for microfabrication. *Microelectron Eng* 1997;35:367–72.
- [16] Adams DP, Vasile M, Benavides G, Campbell A. Micromilling of metal alloys with focused ion beam-fabricated tools. *Prec Eng* 2001;25:107–13.
- [17] Adams DP, Vasile M, Krishnan A. Microgrooving and microthreading tools for fabricating curvilinear features. *Prec Eng* 2000;24:347–56.
- [18] Adams DP, Vasile M, Picard Y. Focused ion beam shaped micro-cutting tools for fabricating curvilinear features. *ASPE Proc* 2000;22:176.
- [19] Harriott L. A second generation focused ion beam micromachining system. *Proc SPIE* 1987;773:190.
- [20] Vasile M, Biddick C, Schwalm S. Microfabrication by ion milling: the lathe technique. *J Vac Sci Technol B* 1994;12:2388.
- [21] Adams DP, Mayer TM, Vasile MJ, submitted for publication.

- [22] Bradley RM, Harper James ME. Theory of ripple topography induced by ion bombardment. *J Vac Sci Technol A* 1988;6(4):2390–5.
- [23] Carter G. The effects of surface ripples on sputtering erosion rates and secondary ion emission yields. *J Appl Phys* 1999;85(1):455–9.
- [24] Klein J, Guckel H. High winding density micro coils for magnetic actuators. *Microsyst Technol* 1998;4:172–5.
- [25] Christenson TR, Klein J, Guckel H. An electromagnetic micro dynamometer. In: *Proceedings of the IEEE MEMS, Amsterdam, the Netherlands; 1995*, p. 386–91.
- [26] Rogers JA, Jackman RJ, Whitesides GM. Constructing single- and multiple-helical microcoils and characterizing their performance as components of microinductors and microelectromagnets. *J Microelectromech Syst* 1997;6(3):184–92.
- [27] Webb AG. Radiofrequency microcoils in magnetic resonance. *Prog Nucl Magn Reson Spectrosc* 1997;31:1–42.
- [28] Becker EW, Ehrfeld W, Hagmann P, Maner A, Münchmeyer D. Fabrication of microstructures with high aspect ratios and great structural heights by synchrotron radiation lithography, galvano-forming, and plastic moulding (LIGA process). *Microelectron Eng* 1986;4:35–56.
- [29] Mahdjour H, Clark WG, Baberschke K. High sensitivity broadband microwave spectroscopy with small non-resonant coils. *Rev Sci Instrum* 1986;57(6):1100–6.
- [30] Dalal HM, Joshi RV, Rathore HS, Phillipi A. A dual damascene hard metal capped Cu and Al alloy for interconnect wiring of ULSI circuits. *Proc Int Electron Dev Mtg* 1993;273–6.
- [31] Orloff J. High-resolution focused ion beams. *Rev Sci Instrum* 1993;64(5):1105–30.
- [32] Russell PE, Stark TJ, Griffis DP, Phillips JR, Jarausck KF. Chemically and geometrically enhanced focused ion beam micromachining. *J Vac Sci Technol B* 1998;16(4):2494–8.